A computational multiscale model of cortical spreading depression propagation

Luca Gerardo-Giorda[1] and Julia M. Kroos[1,*]

[1]BCAM - Basque Center for Applied Mathematics, Bilbao, Spain
[*]Alameda de Mazarredo 14, 48009 Bilbao, Bizkaia, Spain,
jkroos@bcamath.org

December 14, 2016

Abstract

Cortical Spreading Depression (CSD) is a disruption of the brain hemostasis that, originating in the visual cortex and traveling towards the frontal lobe, temporarily impairs the normal functioning of neurons. Although, as of today, little is known about the mechanisms that can trigger or stop such phenomenon, CSD is commonly accepted as a correlate of migraine visual aura. In this paper, we introduce a multiscale PDE-ODE model that couples the propagation of the depolarization wave associated to CSD with a detailed electrophysiological model for the neuronal activity to capture both macroscopic and microscopic dynamics.

Keywords: Cortical Spreading Depression, PDE-ODE coupled systems, finite elements, multiscale modeling **MSC**[2010] 65M60, 92-08, 92C30

1 Introduction

Migraine is a prevailing disease in contemporary society, commonly associated to a number of impairing effects from unilateral severe headache and nausea to photophobia [1]. About one third of migraine patients also experience a migraine aura preceding the typical headache [2, 3]. Several experiments suggest that a propagating depolarization wave on the cerebral cortex is underlying migraine, see [2, 3, 4] and references therein. This wave, named Cortical Spreading Depression (CSD), causes a drastic failure of the brain homeostasis that temporarily impairs the normal functioning of neurons [5, 6]. A key property of neural cells is to produce an action potential (AP), consisting in a sudden increase of the transmembrane potential, called spike, followed by a recovering of the resting condition through a refractory period, during which the cell cannot be excited. The neuronal activity is measured in terms of number of AP produced in one second and is called firing rate (Hz). In the wake of the CSD

propagation wavefront, a complex dynamics is triggered: neurons undergo a brief period of intense firing, followed by a membrane hyperpolarization which silences the spiking activity for a variable period (between 1 and 3 minutes), after which the neurons slowly recover their firing activity and eventually get back to normal frequency (see e.g. [7]). CSD is characterised by relevant increases in both extracellular K^+ and glutamate, as well as rises in intracellular Na^+ and Ca^{2+}, and the two most accepted hypotheses suggest that its propagation is due to diffusion of potassium or glutamate in the extracellular space [8].

Several mathematical tools have been proposed in the past to model CSD, from macroscopic reaction diffusion equations [9] to microscopic biophysical models accounting for specific physiological quantities, such as cells' metabolism [10] or electrodiffusion and osmotic water flow at the tissue level [11]. For a general overview of those models we refer the reader to [8, 12, 13, 14]. Recently, an increasing attention has been paid to the effects of the cortical geometry on CSD propagation, as fissures and sulci of the cortex are expected to influence the propagation of depolarization waves. Pocci and collaborators studied the effect of the cortical bending by using a reaction diffusion equation in a simplified geometry consisting of a 2D duct containing a bend [15], showing how sharp bends naturally block the wave propagation. Dahlem and his collaborators proposed in [16] to use the Gaussian curvature of the cortex (computable from MRI data) to identify potential targets for neuromodulation (see also [17]). The authors of this paper, together with their collaborators, proposed in [18] the use a computational neural firing rate model distributed throughout a realistic cortical mesh reconstructed from MRI, as well as, in [19], a more personalized model where the propagation of potassium wave in the extracellular space was modeled by taking into account diffusion coefficients recovered from Diffusion Tensor Imaging (DTI) data.

As a common trait of the existing literature, biophysical models provide insights on interactions and dynamics at a cellular level, while phenomenological models are more suited for analysing the general CSD propagation. The aim of this paper is to create the first (to the best of our knowledge) bridge between the biophysical and phenomenological modeling approach, in order to provide a deeper understanding of the complex dynamics that are triggered by the passage of the depolarization wave.

Following the potassium assumption for the CSD, we introduce a multiscale coupled PDE-ODE model to deal with both the macroscopic propagation of the depolarization wave and the microscopic neuronal dynamics. The coupled problem is inherently multiscale in time, as CSD propagates very slowly across the cortex (around 20 minutes from back to front), while the electrophysiological dynamics features a way faster temporal scale (in the order of the millisecond). At the macroscopic level, we model the extracellular potassium bath concentration with a modification of the distributed FitzHugh-Nagumo type model proposed by the authors and their collaborators in [19]. The dynamics of the extracellular potassium bath concentration is then used as a driver for the activity of a detailed microscopic electrophysiological model for the neurons. Among the various neuronal models available in literature (see, e.g., [20, 21, 22]), the

microscopic electrophysiological model we build our model upon is the one introduced by Wei et al. [23]. As all the electrophysiological models available in literature describe the behaviour of a single cell, the microscopic component of the coupled model can be considered a nonstandard (with respect to the classical definitions [24]) mean field model. The microscopic variables in a given point $x \in \Omega$ represent the average values of the corresponding quantities for the ensemble of neurons that are physically present in the spatial location at hand. In addition, the use of an ensemble model in space allows, once applied on a geometry reconstructed from medical imaging, to use a computational grid whose characteristic size is of the order of millimeters, the standard resolution of common MRI scanners.

The paper is organised as follows. In section 2 we describe the microscopic electrophysiological model and the macroscopic propagative one. In section 3 the multiscale coupling and its numerical approximation is described. Section 4 is devoted to numerical experiments in both one and two dimensions to illustrate the features of the model.

2 A multiscale distributed model of Cortical Spreading Depression

Cortical Spreading Depression is a disruption of the brain hemostasis that temporarily impairs the normal functioning of neurons and propagates across the cerebral cortex. In the wake of the propagation wavefront a complex dynamics is triggered. At first neurons undergo a brief period of intense activity, exhibiting a firing rate 10-20 times higher than the one at rest (between 8 and 12Hz, see [25, 26]). This brief period of intense excitations is followed by a membrane hyperpolarization which silences the spiking activity for a variable period (between 1 and 3 minutes), after which the neurons slowly recover their spiking activity and eventually get back to normal spiking frequency (see e.g. [7]). Four hypothesis to explain the CSD propagation on the cortex have been proposed, and the two most accepted ones suggest that CSD propagates due to diffusion of potassium or glutamate in the extracellular space, which is presumed to follow ordinary diffusion laws [8]. Differently from what happens in modeling cardiac electrophysiology (see, among others, [27, 28] for an overview of the topic), setting up a distributed model for the membrane potential would not be effective in the description of CSD. Distributed models in cardiac electrophysiology describe the propagation of AP along a cardiac fibre. In the CSD case, we aim at describing the changes in the neuronal activity that are driven by the depolarization wave, and not the synaptic signaling. In this paper we follow the potassium assumption in describing the propagation of the homeostatic disturbance at the cortical level, and we couple it with a detailed microscopic description of the neuronal dynamics. The microscopic electrophysiological model we build our model upon is the one introduced by Wei et al. [23]. At the macroscopic level, we model the extracellular potassium wave with a modification of the FitzHugh-

Nagumo type model proposed by the authors and their collaborators in [19]. In the rest of section we describe the two models in detail.

2.1 Wei's neuronal model

The model introduced by Wei et al. [23] is an extension of the neural model proposed in [21], accounting for a wider range of neuronal activities than the original one. Wei's model supports various behaviours from seizure to spreading depression, tonic firing and a steady state, whose occurrence depends on the values of potassium and oxygen bath concentrations, denoted by k_{bath} and O_{bath}, respectively. A detailed analysis of the bifurcation parameters can be found in [23]. For the sake of completeness, we give here a brief summary of the model, whose parameters are collected in Table 1.

2.1.1 Membrane potential dynamics

The membrane potential V is described by Hodgkin-Huxley type equations:

$$\begin{aligned} C\frac{dV}{dt} &= -I_{\mathrm{Na}} - I_{\mathrm{K}} - I_{\mathrm{Cl}} - \frac{I_{pump}}{\gamma} \\ I_{\mathrm{Na}} &= G_{\mathrm{Na}} m^3 h (V - V_{\mathrm{Na}}) + G_{\mathrm{Na},L}(V - E_{\mathrm{Na}}) \\ I_{\mathrm{K}} &= G_{\mathrm{K}} n^4 (V - V_K) + G_{\mathrm{K},L}(V - E_{\mathrm{K}}) \\ I_{\mathrm{Cl}} &= G_{\mathrm{Cl},L}(V - V_{\mathrm{Cl}}) \\ \frac{dq}{dt} &= \alpha_q(1-q) - \beta_q q, \qquad \text{for } q \in \{m, h, n\}, \end{aligned} \tag{1}$$

where G_{Na}, and G_K are the maximal conductance of Na^+ and K^+, while $G_{\mathrm{Na},L}$, $G_{\mathrm{K},L}$ and $G_{\mathrm{Cl},L}$ are the leak Na^+, K^+ and Cl^- conductances, respectively; I_{Na} and I_{K} are the Na^+ and K^+ currents (including also their respective leak currents) and I_{Cl} is the Cl^- leak current; I_{pump} is the current of the neuronal ATP-dependent Na^+/K^+ pump, that will be described in detail in the next section. Finally, $\gamma = S/(Fv_i)\cdot 10^{-2}$ is a conversion factor from the current units (μA/cm^2) into the concentration units (mM/s), where S is the cell surface, v_i the intracellular volume and $F = 96.485$ C/mol the Faraday constant.
The activation and inactivation variables $q \in \{m, h, n\}$ represent the percentage of ion selective channels in the opened and closed state and vary between 0 and 1 (0 denoting a closed channel, and 1 denoting an open one). Their saturation functions α_q and β_q, $q \in \{m, h, n\}$, are thus voltage-depending opening and closing rates:

$$\alpha_m = 0.32\,\frac{V+54}{1-\exp\left(-\frac{V+54}{4}\right)} \quad \alpha_h = 0.128\,\exp\left(-\frac{V+50}{18}\right) \quad \alpha_n = 0.032\,\frac{V+52}{1-\exp\left(-\frac{V+52}{5}\right)}$$

$$\beta_m = 0.28\,\frac{V+27}{\exp\left(\frac{V+27}{5}\right)-1} \qquad \beta_h = \frac{4}{1+\exp\left(-\frac{V+27}{5}\right)} \qquad \beta_n = 0.5\,\exp\left(-\frac{V+57}{40}\right).$$

The reversal potentials of Na^+, K^+ and Cl^- are linked to the ion concentra-

tions via the Nerst equation:

$$V_{\mathrm{Na}} = 26.64 \ln\left(\frac{[\mathrm{Na}^+]_o}{[\mathrm{Na}^+]_i}\right) \quad V_{\mathrm{K}} = 26.64 \ln\left(\frac{[\mathrm{K}^+]_o}{[\mathrm{K}^+]_i}\right) \quad V_{\mathrm{Cl}} = 26.64 \ln\left(\frac{[\mathrm{Cl}^-]_i}{[\mathrm{Cl}^-]_o}\right)$$

where $[\cdot]_i$ and $[\cdot]_o$ represent intracellular and extracellular concentrations.

2.1.2 Ion concentrations

The concentrations dynamics are governed by the combined action of ionic currents and fluxes. In order to take into account the possibile swelling of the cell during activity, such quantities are computed through the number of ions per volume component, that we denote by

$$N_{\mathrm{X}_i} = v_i[\mathrm{X}]_i, \qquad N_{\mathrm{X}_o} = v_o[\mathrm{X}]_o, \qquad X \in \{\mathrm{Na}^+, \mathrm{K}^+, \mathrm{Cl}^-\}$$

v_i and v_o being the intracellular and extracellular volumes, respectively.
In the intracellular space, their dynamics reads

$$\begin{aligned}
\frac{d}{dt} N_{\mathrm{K}_i^+} &= \frac{1}{\sigma}(-\gamma I_{\mathrm{K}} + 2I_{pump} - I_{kcc2} - I_{nkcc1})v_i \\
\frac{d}{dt} N_{\mathrm{Na}_i^+} &= \frac{1}{\sigma}(-\gamma I_{\mathrm{Na}} - 3I_{pump} - I_{nkcc1})v_i \\
\frac{d}{dt} N_{\mathrm{Cl}_i^-} &= \frac{1}{\sigma}(\gamma I_{\mathrm{Cl},L} - I_{kcc2} - 2I_{nkcc1})v_i,
\end{aligned} \tag{2}$$

while in the extracellular space we have

$$\begin{aligned}
\frac{d}{dt} N_{\mathrm{K}_o^+} &= \frac{1}{\sigma}(\gamma\beta I_{\mathrm{K}} - 2\beta I_{pump} - I_{diff} - I_{glia} - 2I_{gliapump} + \beta I_{kcc2} + \beta I_{nkcc1})v_o \\
\frac{d}{dt} N_{\mathrm{Na}_o^+} &= \frac{1}{\sigma}(\gamma\beta I_{\mathrm{Na}} + 3\beta I_{pump} + \beta I_{nkcc1})v_o \\
\frac{d}{dt} N_{\mathrm{Cl}_o^-} &= \frac{1}{\sigma}(-\gamma\beta I_{\mathrm{Cl},L} + \beta I_{kcc2} + 2\beta I_{nkcc1})v_o.
\end{aligned} \tag{3}$$

In the above equations, $\sigma = 1000$ is the conversion factor from seconds to milliseconds, and $\beta = v_i/v_o$ is the ratio between intracellular and extracellular volume. By letting

$$N_i(t) = \begin{bmatrix} N_{\mathrm{K}_i^+}(t) \\ N_{\mathrm{Na}_i^+}(t) \\ N_{\mathrm{Cl}_i^-}(t) \end{bmatrix} \qquad N_o(t) = \begin{bmatrix} N_{\mathrm{K}_o^+}(t) \\ N_{\mathrm{Na}_o^+}(t) \\ N_{\mathrm{Cl}_o^-}(t) \end{bmatrix},$$

the intracellular and extracellular ion concentrations can be gathered as

$$C_i(t) = \frac{N_i(t)}{v_i(t)}, \qquad C_o(t) = \frac{N_o(t)}{v_o(t)}.$$

In equations (2) and (3), I_{pump} is the neuronal $\mathrm{Na}^+/\mathrm{K}^+$ pump current, I_{diff} is the K^+ diffusion current, I_{glia} is the current associated with the glial buffering,

$I_{gliapump}$ is the glial Na^+/K^+ pump current. Their formulations extend the ones introduced in [21] to include an oxygen dependency:

$$\begin{aligned} I_{pump} &= \frac{\rho([O_2]_o)}{1+\exp((25-[Na^+]_i)/3)} \cdot \frac{1}{1+\exp(3.5-[K^+]_o)} \\ I_{gliapump} &= \frac{1}{3}\frac{\rho([O_2]_o)}{1+\exp((25-[Na^+]_{gi})/3)} \cdot \frac{1}{1+\exp(3.5-[K^+]_o)} \\ I_{glia} &= \frac{G_{glia}(O_{bath})}{1+\exp((18-[K^+]_o)/2.5)} \\ I_{diff} &= \varepsilon_k(\beta, O_{bath})\,([K^+]_o - k_{bath}). \end{aligned} \tag{4}$$

In the above expressions, k_{bath} represents the bath potassium concentration, O_{bath} the bath oxygen concentration, while $[Na^+]_{gi}$ is the intracellular sodium concentration in the glia compartment, that is assumed to be constant. As neural activity consumes the most energy in the brain, the cost of pumps and currents in (4) can be used to estimate the oxygen consumption. In addition, the diffusion of K^+ to the blood is constrained by the instantaneous volume fraction β. The dependence of the Na^+/K^+ ATP pump rate $\rho([O_2]_o)$, the K^+ uptake of the glial cells $G_{glia}(O_{bath})$, and potassium diffusion coefficient $\varepsilon_k(\beta, O_{bath})$ on the available oxygen in the extracellular space is expressed as

$$\begin{aligned} \rho([O_2]_o) &= \frac{\rho_{max}}{1+\exp((20-[O_2]_o)/3)} \\ G_{glia}(O_{bath}) &= \frac{G_{glia,max}}{1+\exp((2.5-O_{bath})/0.2)} \\ \varepsilon_k(\beta, O_{bath}) &= \frac{1}{1+\exp((-20+\beta)/2)} \times \frac{\varepsilon_{k,max}}{1+\exp(2.5-O_{bath})/0.2)}. \end{aligned} \tag{5}$$

The oxygen concentration in the extracellular space, $[O_2]_o$ is assumed to be supplied diffusively by the bath solution O_{bath}, and its dynamics is modeled as

$$\frac{d[O_2]_o}{dt} = \frac{1}{\sigma}\left(-\alpha(I_{pump}+I_{gliapump}) + \varepsilon_0(O_{bath}-[O_2]_o)\right),$$

where ε_0 is the diffusion constant, while α is a conversion factor from the pump current (mM/s) to the oxygen concentration change ($\mathrm{mg\,L^{-1}s^{-1}}$).

Finally, the chloride homeostasis is mainly regulated by cation-chloride co-transporters, in particular by the $Na^+/K^+/2Cl^-$ (NKCC1) and the K^+/Cl^- (KCC2) co-transporters (see [23] for detailed physiological description). The

co-transporter currents I_{nkcc1} and I_{kcc2} are modeled in a Nerst-like form as

$$\begin{aligned} I_{kcc2} &= U_{kcc2} \ln\left(\frac{[\mathrm{K}^+]_i[\mathrm{Cl}^-]_i}{[\mathrm{K}^+]_o[\mathrm{Cl}^-]_o}\right) \\ I_{nkcc1} &= U_{nkcc1} f\left([\mathrm{K}^+]_o\right)\left(\ln\left(\frac{[\mathrm{K}^+]_i[\mathrm{Cl}^-]_i}{[\mathrm{K}^+]_o[\mathrm{Cl}^-]_o}\right) + \ln\left(\frac{[\mathrm{Na}^+]_i[\mathrm{Cl}^-]_i}{[\mathrm{Na}^+]_o[\mathrm{Cl}^-]_o}\right)\right) \\ f([\mathrm{K}^+]_o) &= \frac{1}{1+\exp(16-[\mathrm{K}^+]_o)}, \end{aligned}$$

where U_{kcc2} and U_{nkcc1} are the co-transporter strength.

2.1.3 Volume dynamics

As the cell volume varies according to the level of activity (entailing high ion influx or efflux), the intracellular neuronal volume $\hat{v}_i$ depends on the difference between the extracellular and the intracellular osmotic pressures π_o and π_i: both the extracellular and intracellular fluids consist of water, sodium ions (Na^+), potassium ions (K^+), chloride ions (Cl^-) and negatively charged proteins (A^-) that cannot permeate the membrane, and we have

$$\begin{aligned} \pi_o &= [\mathrm{Na}^+]_o + [\mathrm{K}^+]_o + [\mathrm{Cl}^-]_o + [A^-]_o \\ \pi_i &= [\mathrm{Na}^+]_i + [\mathrm{K}^+]_i + [\mathrm{Cl}^-]_i + [A^-]_i, \end{aligned}$$

where $[A^-]_i = 132\mathrm{mM}$ and $[A^-]_o = 18\mathrm{mM}$ are the intra- and extracellular concentration of anions.

The expected intracellular volume is given by

$$\hat{v}_i = v_i^0 \times \left(1.1029 - 0.1029 \exp\left(\frac{\pi_o - \pi_i}{20}\right)\right), \tag{6}$$

whereas the change of cell volume is defined as

$$\frac{dv_i}{dt} = \frac{\hat{v}_i - v_i}{250}. \tag{7}$$

Assuming a constant total volume, the extracellular volume is computed as

$$v_o = \left(1 + \frac{1}{\beta_0}\right) v_i^0 - v_i, \tag{8}$$

where β_0 is the initial ratio of intra- and extracellular volume, v_i^0 is the initial intracellular volume of a cell with radius 7 μm. The instantaneous volume ratio $\beta = v_i/v_0$ is updated accordingly.

2.1.4 Vectorial representation

In order to simplify the notations, we introduce here a compact vector representation of the Wei's model described in the previous section, and we let

$$N(t) = \begin{bmatrix} N_i(t) \\ N_o(t) \end{bmatrix} \in \mathbb{R}^6, \qquad q(t) = [\, h(t),\ m(t),\ n(t)\,]^T \in \mathbb{R}^3.$$

Furthermore, by setting

$$\Lambda(t) = \begin{bmatrix} v_i(t)\,\mathbb{I}_3 & 0 \\ 0 & v_o(t)\,\mathbb{I}_3 \end{bmatrix} \in \mathbb{R}^{6\times 6},$$

where $\mathbb{I}_3$ is the identity matrix in $\mathbb{R}^3$, we have

$$C(t) = \begin{bmatrix} C_i(t) \\ C_o(t) \end{bmatrix} = \Lambda(t)^{-1} N(t) \in \mathbb{R}^6.$$

By introducing the vectorial notations

$$U(t) = \begin{bmatrix} V(t) \\ q(t) \\ N(t) \\ [\mathrm{O_2}]_\mathrm{o}(t) \\ v_i(t) \end{bmatrix} \in \mathbb{R}^{12}, \qquad W(t) = \begin{bmatrix} C(t) \\ v_o(t) \end{bmatrix} \in \mathbb{R}^7, \tag{9}$$

and by letting

$$\Phi_U(U,W) = \begin{bmatrix} \Phi_V \\ \Phi_q \\ \frac{1}{\sigma}\,\Lambda\,\Phi_N \\ \frac{1}{\sigma}\,\Phi_{O_2} \\ \Phi_{v_i} \end{bmatrix} \in \mathbb{R}^{12}, \quad \Phi_W(U) = \begin{bmatrix} \Lambda^{-1} N \\ \left(1 + \dfrac{1}{\beta_0}\right) v_i^0 - v_i \end{bmatrix} \in \mathbb{R}^7$$

where

$$\Phi_V = -I_\mathrm{Na} - I_\mathrm{K} - I_\mathrm{Cl} - \frac{I_{pump}}{\gamma}, \qquad \Phi_q = \begin{bmatrix} \alpha_h(1-h) - \beta_h h \\ \alpha_m(1-m) - \beta_m m \\ \alpha_n(1-n) - \beta_n n \end{bmatrix},$$

$$\Phi_N = \begin{bmatrix} -\gamma I_\mathrm{K} + 2I_{pump} - I_{kcc2} - I_{nkcc1} \\ -\gamma I_\mathrm{Na} - 3I_{pump} - I_{nkcc1} \\ \gamma I_{\mathrm{Cl},L} - I_{kcc2} - 2I_{nkcc1} \\ \gamma\beta I_\mathrm{K} - 2\beta I_{pump} - I_{diff} - I_{glia} - 2I_{gliapump} + \beta I_{kcc2} + \beta I_{nkcc1} \\ \gamma\beta I_\mathrm{Na} + 3\beta I_{pump} + \beta I_{nkcc1} \\ -\gamma\beta I_{\mathrm{Cl},L} + \beta I_{kcc2} + 2\beta I_{nkcc1} \end{bmatrix},$$

$$\Phi_{O_2} = -\alpha(I_{pump} + I_{gliapump}) + \varepsilon_0([O_2]_{bath} - [O_2]_o), \qquad \Phi_{v_i} = \frac{\hat{v_i} - v_i}{250},$$

we can represent Wei's differential-algebraic system in compact form as

$$\begin{cases} \dfrac{dU}{dt} &= \Phi_U(U, W, k_{bath}) \\ W &= \Phi_W(U). \end{cases} \tag{10}$$

In the above equation we indicate explicitly the dependence of the differential part of the system on the k_{bath}, as we model its variation as the driver for the Cortical Spreading Depression. According to the bifurcation diagram presented in [23], a resting state featuring a spiking frequency around 10-12 Hz is obtained for the parameter choices $k_{bath} = 5.5$ mM and $O_{bath} = 30$ mM, while a spreading depression behaviour is triggered by a higher k_{bath} concentration, in the specific $k_{bath} = 64$, provided $G_{\mathrm{Na},L}$ is doubled with respect to the original paper.

Parameter	Value	Unit	Description
C	1	μF/cm^2	Membrane capacity of the lipid bilayer
G_{Na}	30	mS/cm^2	Maximal conductance of sodium current
G_{K}	25	mS/cm^2	Maximal conductance of potassium current
$G_{\mathrm{Na},L}$	0.0247	mS/cm^2	Conductance of leak sodium current
$G_{\mathrm{K},L}$	0.05	mS/cm^2	Conductance of leak potassium current
$G_{\mathrm{Cl},L}$	0.1	mS/cm^2	Conductance of leak chloride current
β_0	7		Initial ratio between intra- and extracellular volume
ρ_{max}	0.8	mM/s	Maximal Na^+/K^+ pump rate
$\varepsilon_{k,max}$	0.25	s^{-1}	Maximal potassium diffusion rate
$G_{glia,max}$	5	mM/s	Maximal glial uptake strength of potassium
$[\mathrm{K}^+]_{bath}$	3.5	mM	Normal bath potassium concentration
ε_0	0.17	s^{-1}	Oxygen diffusion rate
$[\mathrm{Na}^+]_{gi}$	18	mM	Glial intracellular sodium concentration
α	5.3	g/mol	conversion factor
$[O_2]_{bath}$	32	mg/L	Normal bath oxygen concentration
U_{kcc2}	0.3	mM/s	Maximal KCC2 cotransporter strength
U_{nkcc1}	0.1	mM/s	Maximal NKCC1 cotransporter strength
σ	1000	s	Conversion from seconds to miliseconds
D	3.8 $\times 10^{-5}$	mm^2/s	Diffusion coefficient of k_{bath}
k_0	5.5	mM	resting value of k_{bath} concentration
k_{th}	11.8	mM	threshold parameter
k_p	64	mM	peak value
η_1	2.6	s^{-1}	
η_2	200	s^{-1}	
η_3	1×10^{-5}	s^{-1}	
η_4	60	mM^{-1} s^{-1}	

Table 1: Description, units and values of the model parameters.

2.2 Propagation of the depolarization wave

The cortical spreading depression is following a propagative disruption of the brain hemostasis. To model the propagation of the depolarisation wave we consider the extracellular bath potassium concentration (k_{bath}) as the propagating agent. Following [18, 19], we model the k_{bath} propagation with a coupled reaction-diffusion PDE/ODE model

$$
\begin{aligned}
\frac{\partial k_{bath}}{\partial t} &= \operatorname{div}\left(D\nabla k_{bath}\right) - F(k_{bath}, w) \\
\frac{\partial w}{\partial t} &= G(k_{bath}, w) \\
F(k_{bath}, w) &= \eta_1 \left(k_{bath} - k_0\right) \left(1 - \frac{k_{bath}}{k_{th}}\right) \left(1 - \frac{k_{bath}}{k_p}\right) + \eta_2 \left(k_{bath} - k_0\right) w \\
G(k_{bath}, w) &= \eta_3 \left(k_{bath} - k_0 - \eta_4 w\right),
\end{aligned}
\tag{11}
$$

where D is the diffusion tensor, w is a recovery variable, η_1, η_2, η_3, and η_4 are parameters, while k_0, k_{th}, k_p are the resting, threshold, and peak values of the k_{bath} concentration, respectively. System (11) is a modified version of the Roger-McCulloch variant [29] to the Fitzhugh-Nagumo model [30]: the plateau duration has been tuned in order for the Wei model described in the previous section to reproduce the characteristic neuronal activation state during CSD, with a resting condition around 12Hz, a brief period of intense firing in the excited state, and a silencing period matching the duration of the neuron activity disruption that follows the passage of the CSD (a few minutes, [7]). The coupled PDE-ODE problem (11) is set on a computational domain $\Omega \times (0, T)$, $\Omega \subset \mathbb{R}^d$ ($d = 1, 2, 3$). A mathematically well posed problem is obtained by imposing initial conditions $k^0_{bath}(x) = k_{bath}(0, x)$ and $w^0(x) = w(0, x)$ in Ω and suitable boundary conditions on $\partial\Omega$: homogeneous Neumann boundary conditions are imposed to model an isolated environment.

2.2.1 Numerical approximation

We discretise problem (11) by finite elements in space and finite differences in time. Let $\mathcal{T}_h$ be a regular triangulation of $\Omega \subset \mathbb{R}^d$ ($d = 1, 2, 3$), namely $\Omega = \bigcup_{j=1}^{N} K_j$, where each $K_j \in \mathcal{T}_h$ is the image of the reference element E, through an invertible affine map T_{K_j} ($K_j = T_{K_j}(E)$). We define h as the maximum diameter of the elements of the triangulation. The associated finite element spaces X^k_h (see e.g. [31] for an introduction to finite element methods) is defined as

$$
X^k_h = \left\{ \varphi_h \in C^0(\Omega) \,|\, \varphi_{h|K_j} \circ T_{K_j} \in \mathbb{P}_k(E) \right\},
$$

where $\mathbb{P}_k(E)$ is the space of polynomials of degree at most k on E. In the numerical simulation presented in this paper we use piecewise linear ($k = 1$) elements.

A semi-discrete problem in space is then obtained by applying a Galerkin procedure, using as finite dimensional space $V_h = X^k_h$, and choosing a basis for V_h. By letting $\{\varphi_i\}_{i=1,..,N_h}$ be the finite element basis, the semi-discrete

unknowns are thus given by

$$k_{bath}(x,t) = \sum_{i=1}^{N_h} \boldsymbol{k}_i(t)\varphi(x) \qquad\qquad w(x,t) = \sum_{i=1}^{N_h} \boldsymbol{w}_i(t)\varphi(x).$$

We define the semi-discrete unknown vectors $\boldsymbol{k}_{bath} = [\boldsymbol{k}_1(t), \ldots, \boldsymbol{k}_{N_h}(t)]^T$ and $\boldsymbol{w} = [\boldsymbol{w}_1(t), \ldots, \boldsymbol{w}_{N_h}(t)]^T$, and we introduce the symmetric mass, $M = (m_{kl})$, and stiffnes, $S = (s_{kl})$, matrices, defined as

$$m_{kl} = \sum_{j=1}^{N} \int_{K_j} \varphi_k \varphi_l \, dx \qquad\qquad s_{kl} = \sum_{j=1}^{N} \int_{K_j} (\nabla\varphi_k)^T D(x) \nabla\varphi_l \, dx.$$

Numerical evaluation of the above integrals is obtained by means of a suitable quadrature rule.

With these positions, the finite elements approximation of equation (11) is the solution of

$$M\frac{d\boldsymbol{k}_{bath}}{dt} + S\boldsymbol{k}_{bath} + M\,F(\boldsymbol{k}_{bath}, \boldsymbol{w}) = \boldsymbol{0}, \tag{12}$$

coupled with the semi-discrete formulation of the dynamics of the recovery variable

$$\frac{d\boldsymbol{w}}{dt} = G(\boldsymbol{k}_{bath}, \boldsymbol{w}). \tag{13}$$

A fully discrete approximation of the problem is then obtained by integrating system (12)-(13) in time. For the sake of simplicity in presentation, we consider a fixed time step Δt, although time adaptive scheme can be considered as well. Let thus $t^n = n\Delta t$, for $n = 0, \ldots, N_t$, be a discretisation of the time interval $(0, T)$: we denote with superscript n the variables computed at time t^n. With these positions, we integrate in time system (12)-(13) by means of a mixed implicit/explicit (IMEX) scheme: the linear diffusion term is discretized implicitly, while the nonlinear reaction term $F(\boldsymbol{k}_{bath}, \boldsymbol{w})$ is treated explicitly. The mass matrix M can be lumped to diagonal form by standard techniques. Owing to its peculiar form, the ODE for the recovery variable can be linearised around $\boldsymbol{k}_{bath}$ at the previous time step, and integrated exactly on $(0, \Delta t)$.

This allows us to decouple the PDE-ODE system by solving with respect to the recovery variable $\boldsymbol{w}^{n+1}$ first, given the potassium bath at the previous time step $\boldsymbol{k}^n_{bath}$, and then solving for $\boldsymbol{k}^{n+1}_{bath}$

$$M\frac{\boldsymbol{k}^{n+1}_{bath} - \boldsymbol{k}^n_{bath}}{\Delta t} + S\boldsymbol{k}^{n+1}_{bath} + M\,F(\boldsymbol{k}^n_{bath}, \boldsymbol{w}^{n+1}) = \boldsymbol{0}.$$

With this choice (notice that one could solve for $\boldsymbol{k}_{bath}$ first and update successively the recovery variable), the IMEX method to approximate system (12)-(13) requires to solve, at each time step, the linear system

$$(M + \Delta t\, S)\, \boldsymbol{k}^{n+1}_{bath} = M\boldsymbol{k}^n_{bath} - \Delta t\, M\, F(\boldsymbol{k}^n_{bath}, \boldsymbol{w}^{n+1}). \tag{14}$$

3 Multiscale numerical approximation

The Cortical Spreading Depression propagates very slowly across the cortex (around 20 minutes from back to front), while the electrophysiological dynamics features a way faster temporal scale (in the order of the millisecond). As a consequence, the coupled problem is inherently multiscale in time, posing a non negligible computational challenge. The coupled system, given suitable initial conditions (k^0_{bath}, w^0, U^0, W^0) reads as follows:

$$\begin{cases} \dfrac{\partial k_{bath}}{\partial t} &= \operatorname{div}(D\nabla k_{bath}) - F(k_{bath}, w) & \text{in } \Omega \times (0,T) \\ \dfrac{\partial w}{\partial t} &= G(k_{bath}, w) & \text{in } \Omega \times (0,T) \\ \dfrac{1}{\sigma}\dfrac{\partial U}{\partial t} &= \mathbf{\Phi}_U(U, W, k_{bath}) & \text{in } \Omega \times (0,T) \\ W &= \mathbf{\Phi}_W(U) & \text{in } \Omega \times (0,T). \end{cases} \tag{15}$$

In the above system, $F(k_{bath}, w)$ and $G(k_{bath}, w)$ are the ones defined in (11), U and W are defined in (9), while $\sigma = 1000$ is the conversion factor to the temporal scale of the electrophysiology. Due to the multiscale nature of the coupled system, we structure the computations by propagating the systems with different time steps, and synchronising them at the end of each slow time step. We denote by Δt the time step at which we integrate the propagative dynamics, and by $\Delta\tau$ the time step at which we solve the electrophysiology. The system coupling is unidirectional, as there is no feedback from the electrophysiological part to the propagative part of the model. As a consequence, to go from t^n to t^{n+1}, we propagate the pair (k_{bath}, w) along one time step Δt, we interpolate k_{bath} on $(0, \Delta t)$ along the fine temporal scale $\Delta\tau$, and we solve for the electrophysiological variables (U, W). For simplicity in presentation, we assume a constant ratio N_τ between the temporal discretization steps, namely we let $\Delta t = N_\tau \Delta\tau$. A variable ratio, following a time adaptive scheme in both components, can be considered, with a little additional care in the proper choice of the synchronization instants. Let $t^n = n\Delta t$, for $n = 0, \dots, N_t$, be a discretisation of the time interval $(0, T)$. We denote by $\boldsymbol{k}^n_{bath}$ and $\boldsymbol{w}^n$ the approximation of k_{bath} and w at time $t = t^n$, and with $\boldsymbol{U}^{n,m}$ and $\boldsymbol{W}^{n,m}$ $(m = 0, .., N_\tau)$ the approximation of U and W, respectively, at time $t = t^n + m\Delta\tau$. The following pseudocode summarizes the details of the algorithm.

Multiscale coupling Algorithm

Initialize

$$\boldsymbol{k}_{bath}^0 \in \mathbb{R}^{N_h}, \quad \boldsymbol{w}^0 \in \mathbb{R}^{N_h}, \quad \boldsymbol{U}^{0,0} \in \mathbb{R}^{12\times N_h}, \quad \boldsymbol{W}^{0,0} \in \mathbb{R}^{7\times N_h}$$

for $n = 0, ..., N_t - 1$:

Update $\quad \boldsymbol{w}^{n+1} = \dfrac{\boldsymbol{k}_{bath}^n - k_0}{\eta_4} + \left(\boldsymbol{w}^n - \dfrac{\boldsymbol{k}_{bath}^n - k_0}{\eta_4}\right) \exp\left(-\eta_3\eta_4\Delta t\right)$

Update $\quad F_h^{n+1} = F(\boldsymbol{k}_{bath}^n, \boldsymbol{w}^{n+1})$

Solve $\quad (M + \Delta t\, S)\ \boldsymbol{k}_{bath}^{n+1} = M\boldsymbol{k}_{bath}^n - \Delta t M F_h^{n+1}.$

Interpolate between $\boldsymbol{k}_{bath}^{n-1}$ and $\boldsymbol{k}_{bath}^n$ on $(0, \Delta t)$ at $m\,\Delta\tau$:

$$\boldsymbol{k}_{bath}^{n,m} = \left(1 - \frac{m\Delta\tau}{\Delta t}\right) \boldsymbol{k}_{bath}^{n-1} + \frac{m\Delta\tau}{\Delta t}\, \boldsymbol{k}_{bath}^n \qquad \text{for } m = 1, ..N_\tau$$

for $m = 1, ..., N_\tau$:

Solve $\quad \dfrac{\boldsymbol{U}^{n,m} - \boldsymbol{U}^{n,m-1}}{\Delta\tau} = \Phi_U(\boldsymbol{U}_h^{n,m-1}, \boldsymbol{W}^{n,m-1}, \boldsymbol{k}_{bath}^{n,m})$

Update $\quad \boldsymbol{W}^{n,m} = \Phi_W(\boldsymbol{U}^{n,m})$

end

end

For the sake of simplicity in the above pseudocode description, the time integrator for the ODE system of electrophysiology is a Forward Euler method for $\boldsymbol{U}^{n,m}$ coupled with a linearization around the previous state of the algebraic unknowns $\boldsymbol{W}^{n,m-1}$, but other options (such as Backward Euler, Crank-Nicholson, Runge-Kutta, or Multistep) are available, and can be further explored in order to improve computational efficiency. If the temporal discretization is implicit, one step of a Newton method is required to actually compute $\boldsymbol{U}^{n,m}$. This is not the case for an explicit temporal discretization, but in that situation the stiffness of the ODE system would rule the choice of the time step for the electrophysiology.

4 Numerical simulations

In this section, to illustrate the model features, we present the numerical simulation of a CSD propagation in a one dimensional and a two dimensional domain. The numerical simulations of the multiscale coupled model are performed with a self-developed code in Matlab (MathWorks Inc., Natick, MA), where we chose a constant time step $\Delta t = 0.05\,\mathrm{s}$ for the propagation, and a constant time step $\Delta\tau = 0.05\,\mathrm{ms}$ for the electrophysiology, resulting in performing $N_\tau = 1000$ elec-

trophysiology steps within a propagative time step. The IMEX scheme described in Sections 2.2.1 and 3 requires to solve a linear system associated with a linear parabolic system, for which a vast literature on preconditioning is available [32]. The associated finite element matrix being symmetric, we solve system (14) with a Conjugate Gradient (CG) method, preconditioned by Incomplete Choleski factorization (IC), with pivoting and drop tolerance set at 10^{-6}. Since the coefficients do not change in time during the simulation, so does the finite element matrix in (14): it is thus rentable to implement a low drop tolerance in the IC factorization, as the same preconditioner will be used along the whole CSD propagation. The stopping criterion for CG is set at 10^{-6}, and a maximum number of iteration is set at 60. The combined effect of the low drop tolerance in the IC factorization, and the propagative nature of the solution of system (14) entails that choosing as initial guess, at time t^{n+1}, the solution at previous time step k_{bath}^n, the preconditioned CG converges in very few iterations. The electrophysiology model is solved by an explicit Euler scheme.

Variable	**Value**	**Unit**	**Description**
V	-74.30	mV	membrane potential
v_i	1.4368×10^{-15}	mm^3	intracellular volume
v_o	v_i/β_0	mm^3	extracellular volume
β_0	7		intra-/extracellular volume ratio
$[K^+]_o$	4	mM	extracellular potassium concentration
$[K^+]_i$	140	mM	intracellular potassium concentration
$[Na^+]_o$	144	mM	extracellular sodium concentration
$[Na^+]_i$	18	mM	intracellular sodium concentration
$[Cl^-]_o$	130	mM	extracellular chloride concentration
$[Cl^-]_i$	6	mM	intracellular chloride concentration
$[O_2]_o$	29.3	mM	extracellular oxygen concentration
k_{bath}	64	mM	high bath concentration of potassium
m	0.0031		
h	0.9994		
n	0.0107		
w	0		

Table 2: Initial conditions for the coupled multiscale model.

4.1 Measurable variables

Although the neuronal activity takes place at a millisecond timescale, the whole CSD propagation event occurs at the larger timescale of the minute. In order to be able to grasp the overall dynamics without resorting to the fine timescale of the electrophysiology, we introduce two auxiliary variables allowing to track the depolarisation wave at the time scale of seconds. The first quantity is the

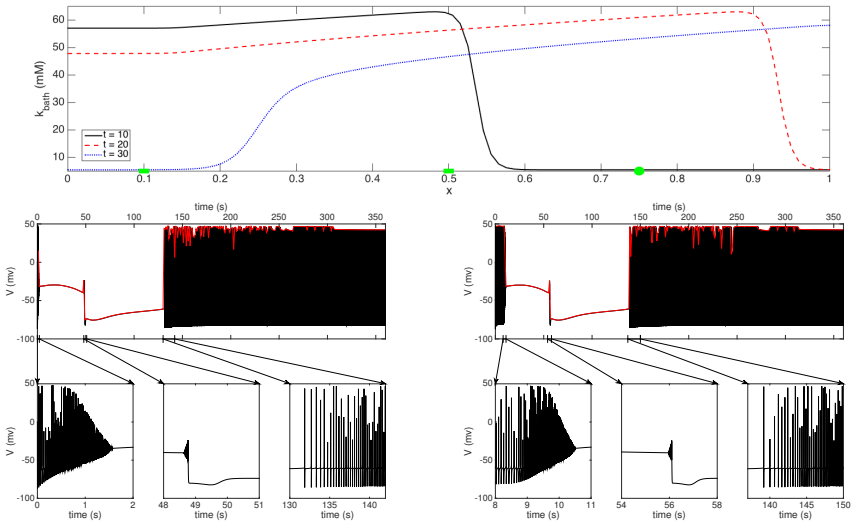

Figure 1: **1D Test. Top:** Profile of k_{bath} at times $t = 10\,\text{s}$, $t = 20\,\text{s}$, and $t = 30\,\text{s}$, and the points $x = 0.1$, $x = 0.5$ (rectangles) and $x = 0.75$ (circle). **Middle:** Temporal dynamics of the membrane potential V (in black) and its maximum V_{max} (in red) at points $x = 0.1$, $x = 0.5$. **Bottom:** Zoom at the regions of intense firing, and slow recovering of firing at the end of the CSD induced activity disruption.

maximum membrane potential in a given point x, defined, at each second t, as

$$V_{max}(x,t) = \max_{s\in[t-1,t]} V(x,s), \tag{16}$$

a commonly measured quantity also by experimentalists (see, e.g., [7, 14]). Another common way to characterise the neuronal activity is through its spiking frequency (in Hz), which is naturally defined at the second timescale. We denote by $\phi(x,t)$ the spiking frequency in a given point x, during the interval $[t-1,t]$.

4.2 1D propagation

In the first example, we consider a one dimensional domain $\Omega = (0,1)$. We consider a uniform diffusion coefficient for k_{bath}, $D = 5 \times 10^{-4}$, as well as homogeneous Neumann boundary conditions to model an isolated environment. We consider a uniform spatial mesh with characteristic size $h = 0.01$, and uniform time steps $\Delta t = 0.05\,\text{s}$ for the propagative part, and $\Delta\tau = 0.05\,\text{ms}$ for the electrophysiology. We initialize the problem by imposing $k_{bath} = 64$ in the left extreme of the interval, and we simulate the propagation of CSD towards the right. The other initial conditions are reported in Table 2.

In Figure 1 (top) we show the propagation in space of k_{bath} by plotting its profile at 3 different time steps ($t = 10\,\text{s}$, $t = 20\,\text{s}$, and $t = 30\,\text{s}$), as well as

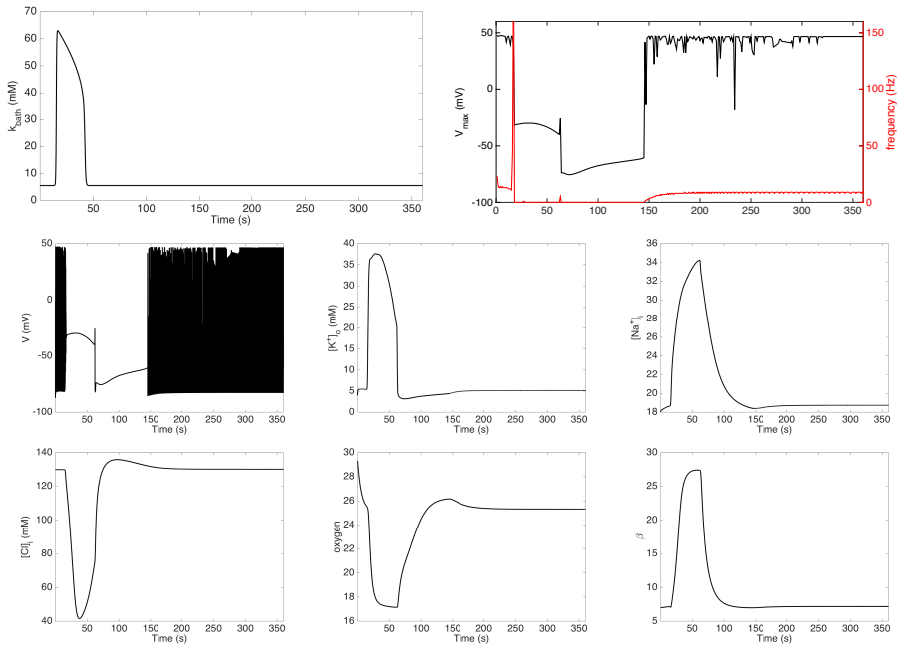

Figure 2: **1D Test.** Temporal dynamics in $x = 0.75$. **Top:** k_{bath}, membrane potential maximum V_{max}, and frequency ϕ. **Middle:** membrane potential V, extracellular potassium $[K^+]_o$, and intracellular sodium $[Na^+]_i$. **Bottom:** intracellular chlorine $[Cl^+]_i$, extracellular potassium $[O_2]_o$, and intra to extracellular volume ratio β.

(middle) the temporal evolution of the membrane potential and its maximum V_{max} in the two points $x = 0.1$ and $x = 0.5$ (identified by green rectangles in the top row). The different times of CSD onset that follow the k_{bath} propagation can be appreciated. We also highlight (bottom) the regions of high, intense, firing that initiates the CSD, and the slow recover of firing activity at the end of the neuronal activity disruption. The silencing period (around 130sec) is compatible with reported values in literature [7, 14].

In Figure 2 we show the temporal evolution of k_{bath}, the maximum membrane potential V_{max}, the spiking frequency ϕ, the membrane potential, the ionic concentrations, oxygen concentration, and intra to extracellular volume ratio β, at point $x = 0.75$ (highlighted by a green circle in Figure 1, top).

4.3 2D propagation

In the second example, we consider as two dimensional domain the unit square $\Omega = (0, 1) \times (0, 1)$. We consider a uniform diffusion coefficient for k_{bath}, $D = 5 \times 10^{-4}$, and homogeneous Neumann boundary conditions. We discretize Ω

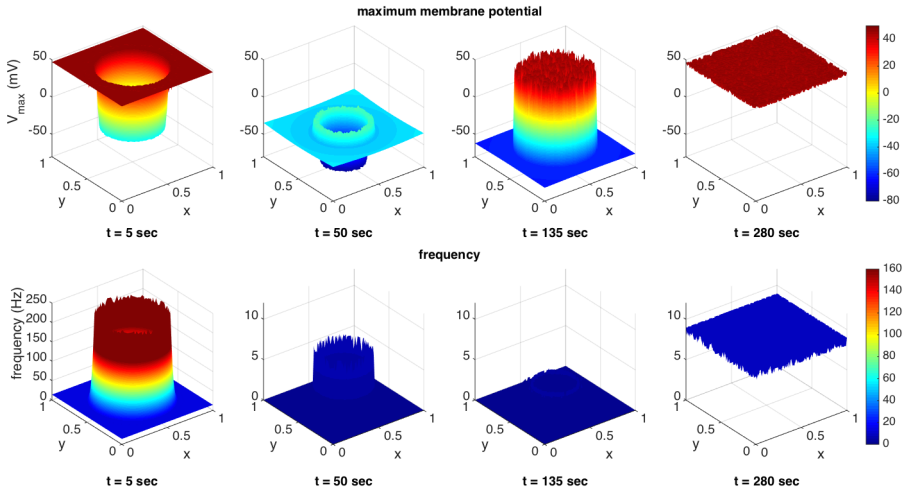

Figure 3: **2D Test.**Temporal evolution of the membrane potential maximum V_{max} and spiking frequency ϕ at times $t = 5\,\mathrm{s}$, t =50 s, t =138 s, and t =280 s.

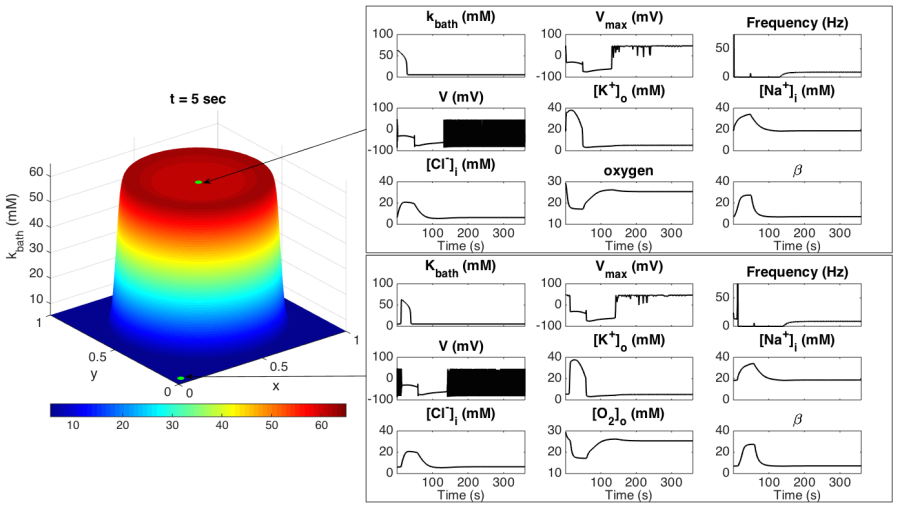

Figure 4: **2D Test.** Profile of k_{bath} at time $t = 5\,\mathrm{s}$, and the temporal evolution of the electrophysiological variables in points $(x, y) = (0.5, 0.5)$ and $(x, y) = (0.05, 0.05)$.

in space with an unstructured mesh with characteristic size $h = 0.01$, and chose uniform time steps for both the propagative part, $\Delta t = 0.05\,\mathrm{s}$, and for

the electrophysiology, $\Delta\tau = 0.05\,\text{ms}$. We simulate a CSD propagating from the center of the domain, where we initially impose $k_{bath} = 64$, and run the simulation for 360 seconds. The other initial conditions are reported in Table 2. In Figure 3 we plot the maximum of the action potential V_{max} and the frequency ϕ at four different times, $t = 5\,\text{s}$, $t = 50\,\text{s}$, $t = 138\,\text{s}$, and $t = 280\,\text{s}$.

In Figure 4, we plot the k_{bath} distribution at $t = 5\,\text{s}$, and the whole temporal dynamics in the points $(x, y) = (0.5, 0.5)$ and $(x, y) = (0.05, 0.05)$.

5 Conclusions

We introduced here a multiscale coupled PDE-ODE model to simulate the propagation of a Cortical Spreading Depression with electrophysiological detail. The electrophysiological model proposed in [23] is paired with the propagative model for the extracellular potassium introduced by the authors in [18, 19]. The detailed description of the electrophysiological activity, provides a major improvement of the modeling accuracy, at the cost of an additional computational effort. The use of more effective ODE solvers within the propagative time steps is anticipated to significantly reduce the computational cost of the overall procedure, and will be investigated. In addition, the proposed model can be extended for tackling more complex problems. CSD has been experimentally demonstrated in animal models, but its evidence in humans is so far limited to indirect assessments, such as the migraine aura itself and a spreading oligemia (a cerebral blood flow reduction observed during the migraine attack, that follows the CSD expected pattern). In this direction, we plan to combine the proposed multiscale model with a metabolic one [33] to gain further insight on the systemic effects of CSD, such as the onset of a lactate wave following its passage, that has been observed in some experimental studies on mice [34].

Acknowledgements This work was supported by the Basque Government through the BERC 2014-2017 program, and by the Spanish Ministry of Economics and Competitiveness MINECO through the BCAM Severo Ochoa excellence accreditation SEV-2013-0323 and the Spanish "Plan Estatal de Investigación, Desarrollo e Innovación Orientada a los Retos de la Sociedad" under Grant BELEMET - Brain ELEctro-METabolic modeling and numerical approximation (MTM2015-69992-R).

References

References

[1] Vos T, Flaxman AD, Naghavi M, Lozano R, Michaud C, Ezzati M, et.al. (2013) Years lived with disability (YLDs) for 1160 sequelae of 289 diseases and injuries 1990?2010: a systematic analysis for the Global Burden of Disease Study 2010. *The Lancet*, 380(9859), 2163-2196.

[2] Hadjikhani N, Sanchez del Rio M, Wu O, Schwartz D, Bakker D, Fischl B, Kwong KK, Cutrer FM, Rosen BR, Tootell RBH, Sorensen AG, Moskowitz, MA. (2001) Mechnisms of migraine aura revealed by functional MRI in human visual cortex. *Proceedings of the National Academy of Sciences of the USA* 98, 4687–4692. DOI: 10.1073/pnas.071582498

[3] Richter F, Lehmenkühler A. (2008). Cortical spreading depression (csd): A neurophysiological correlate of migraine aura. *Der Schmerz* 22, 544–50. DOI: 10.1007/s00482-008-0653-9

[4] de Tommaso M, Ambrosini A, Brighina F, Coppola G, Perrotta A, Pierelli, F., Sandrini, G., Valeriani, M., Marinazzo, D., Stramaglia, S., Schoenen, J. (2014). Altered processing of sensory stimuli in patients with migraine. *Nat Rev Neurol* 10, 144–155

[5] Leão A. (1944). Spreading depression of activity in the cerebral cortex. *J. Neurophysiol.* 7, 391–396

[6] Leão A. (1947). Further observations on the spreading depression of activity in the cerebral cortex. *J. Neurophysiol.* 10, 409–414

[7] Sawant-Pokam PM, Suryavanshi P, Mendez JM, Dudek FE, Brennan KC. (2016) Mechanisms of neuronal Silencing after cortical spreading depression. Cereb Cortex. 1-15. doi: 10.1093/cercor/bhv328.

[8] Zandt B, ten Haken B, van Putten MJAM, Dahlem MA. (2015) How does Spreading Depression Spread? - Physiology and Modeling. Reviews in the Neurosciences. 26(2):183-198. doi: 10.1515/revneuro-2014-0069.

[9] Tuckwell HC, Miura RM. (1978) A mathematical model for spreading cortical depression, *Biophysical J.*; **23(2)**: 257–276, doi: 10.1016/S0006-3495(78)85447-2.

[10] Reggia JA, Montgomery D. (1996) A computational model of visual hallucinations in migraine, *Computers in Biology and medicine*; **26(2)**: 133–141, doi: 10.1016/0010-4825(95)00051-8.

[11] Mori Y. (2015) A multidomain model for ionic electrodiffusion and osmosis with an application to cortical spreading depression. *Physica D: Nonlinear Phenomena*, 308, 94-108.

[12] Somjen GG. (2001) Mechanisms of Spreading Depression and Hypoxic Spreading Depression-Like Depolarization. Physiological Reviews. 81(3): 1065-1096.

[13] Miura RM, Huang H, Wylie JJ. (2013) Mathematical approaches to modeling of cortical spreading depression, *Chaos* **23(4)**, doi: 10.1063/1.4821955.

[14] Pietrobon D, Moskowitz MA. (2014) Chaos and commotion in the wake of cortical spreading depression and spreading depolarisation. Nat Rev Neurosci. 15(6):379-93. doi: 10.1038/nrn3770.

[15] Pocci C, Moussa A, Hubert F, Chapuisat G. (2010) Numerical study of the stopping of aura during migraine, *ESAIM: Proceedings*; **30**: 44–52, doi: 10.1051/proc/2010005.

[16] Dahlem M, Schmidt B, Bojak I, Boie F, Kneer S, Hadjikhani N, Kurths J. (2015). Cortical hot spots and labyrinths: why cortical neuromodulation for episodic migraine with aura should be personalized. *Front Comput Neurosci.* 9. DOI: 10.3389/fncom.2015.00029

[17] Costa C, Tozzi A, Rainero I, Cupini LM, Calabresi P, Ayata C, Sarchielli P. (2013) Cortical spreading depression as a target for anti-migraine agents, *The Journal of Headache and Pain*, 14:62, doi: 10.1186/1129-2377-14-62.

[18] Kroos JM, Diez I, Cortes JM, Stramaglia S, Gerardo-Giorda L. (2016) Geometry Shapes Propagation: Assessing the Presence and Absence of Cortical Symmetries through a Computational Model of Cortical Spreading Depression. *Front. Comput. Neurosci.* 10:6. doi: 10.3389/fncom.2016.00006

[19] Kroos JM, Marinelli I, Diez I, Cortes JM, Stramaglia S, Gerardo-Giorda L. (2017) Patient-specific computational modeling of Cortical Spreading Depression via Diffusion Tensor Imaging *Int. J. Numer. Meth. Biomed. Engng* (to appear)

[20] Izhikevich EM. (2007) Dynamical Systems in Neuroscience: The Geometry of Excitability and Bursting (Computational Neuroscience), *MIT Press* 2007.

[21] Cressman JR Jr, Ullah G, Ziburkus J, Schiff SJ, Barreto E. (2009) The influence of sodium and potassium dynamics on excitability, seizures, and the stability of persistent states: I. Single neuron dynamics. *J Comput Neurosci.* 26(2):159-157. doi: 10.1007/s10827-008-0132-4.

[22] Barreto E, Cressman JR. (2011) Ion concentration dynamics as a mechanism for neuronal bursting, *Journal of Biological Physics* 37 (3) 361–373.

[23] Wei Y, Ullah G, Schiff SJ. (2014) Unification of Neuronal Spikes, Seizure, and Spreading Depression. The Journal of Neuroscience. 34(35):11733-11743. doi: 10.1523/JNEUROSCI.0516-14/2014.

[24] Deco G, Jirsa VK, Robinson PA, Breakspear M, Friston K. (2008) The dynamic brain: from spiking neurons to neural masses and cortical fields. *PLoS Comput Biol.*; 4(8):e1000092.

[25] Hyder F, Fulbright RK, Shulman RG, Rothman DL. (2013) Glutamatergic function in the resting awake human brain is supported by uniformly high oxidative energy. *Journal of Cerebral Blood Flow and Metabolism*, 33(3), 339-347.

[26] Brötzner CP, Klimesch W, Doppelmayr M, Zauner A, Kerschbaum HH. (2014) Resting state alpha frequency is associated with menstrual cycle phase, estradiol and use of oral contraceptives. *Brain research*, 1577, 36-44.

[27] Clayton RH, Bernus OM, Cherry EM, Dierckx H, Fenton FH, Mirabella L, Panfilov AV, Sachse FB, Seemann G, Zhang H. (2011) Models of cardiac tissue electrophysiology: Progress, challenges and open questions. *Progress in Biophysics and Molecular Biology*, 104, pp. 22 – 48.

[28] Sachse FB. (2004) *Computational Cardiology.* Springer, Berlin.

[29] Rogers J, McCulloch A. (1994). A collocation - galerkin finite element model of cardiac action potential propagation. *IEEE Trans Biomed Eng.* 41, 743–757. DOI: 10.1109/10.310090

[30] FitzHugh R. (1961) Impulses and physiological states in theoretical models of nerve membrane. *Biophysical Journal* 1, 445–466

[31] Quarteroni A, Valli A. (1994) *Numerical Approximation of Partial Differential Equations.* Springer-Verlag, Berlin.

[32] Saad Y. (2003). *Iterative methods for sparse linear systems.* SIAM.

[33] Calvetti D, Cheng Y, Somersalo E. (2015) A spatially distributed computational model of brain cellular metabolism, *Journal of theoretical biology* 376, 48–65.

[34] Cruz NF, Adachi K, Dienel GA. (1999) Rapid Efflux of Lactate From Cerebral Cortex During K^+-Induced Spreading Cortical Depression. *Journal of Cerebral Blood Flow and Metabolism.*19(4):380-92.